A dual laser scanning confocal and transmission electron microscopy analysis of the intracellular localisation, aggregation and particle formation of African horse sickness virus major core protein VP7

Running title: Particle formation of modified AHSV protein VP7

Authors: Gayle V. Wall, Daria A. Rutkowska[1], Eshchar Mizrachi, Henk Huismans and Vida van Staden*

Author addresses:

Department of Genetics, University of Pretoria, Pretoria, 0002, South Africa

*Corresponding author: Dr Vida van Staden

E-mail address: vida.vanstaden@up.ac.za

Mailing address: Department of Genetics
University of Pretoria
Private Bag X20
HATFIELD
0028
South Africa

Tel: +27 12 420 3257

Fax: +27 12 362 5327

[1] Present address: Council for Scientific and Industrial Research (CSIR), Biosciences, Pretoria, 0001, South Africa

ABSTRACT

The bulk of African horse sickness virus (AHSV) major core protein VP7 self-assembles into flat, hexagonal crystalline particles in a process appearing unrelated to viral replication. Why this unique characteristic of AHSV VP7 is genetically conserved, and whether VP7 aggregation and particle formation have an effect on cellular biology or the viral life cycle, is unknown. Here we investigated how different small peptide and enhanced green fluorescent protein (eGFP) insertions into the VP7 top domain affected VP7 localisation, aggregation and particle formation. This was done using a dual laser scanning confocal and transmission electron microscopy approach in conjunction with analyses of the solubility, aggregation and fluorescence profiles of the proteins. VP7 top domain modifications did not prevent trimerisation, or intracellular trafficking to one or two discrete sites in the cell. However, modifications that resulted in a misfolded and insoluble VP7-eGFP component blocked trafficking, and precluded protein accumulation at a single cellular site, perhaps by interfering with normal trimer-trimer interactions. Furthermore, the modifications disrupted the stable layering of the trimers into characteristic AHSV VP7 crystalline particles. It was concluded that VP7 trafficking is driven by a balance between VP7 solubility, trimer forming ability and trimer-trimer interactions.

KEY WORDS

AHSV VP7, protein aggregation, particle formation, VP7 localisation, protein solubility.

INTRODUCTION

African horse sickness virus (AHSV) is the causative agent of African horse sickness, an economically important viral disease of *Equidae,* endemic to many areas of sub-Saharan Africa (Mellor & Hamblin 2004). It a member of the *Orbivirus* genus (family *Reoviridae*), of which the closely related bluetongue virus (BTV) is the prototype species (Roy 1996). These viruses are assembled from seven structural proteins (VP1 to VP7), and house a segmented double-stranded RNA (dsRNA) genome (Oellermann et al. 1970; Verwoerd et al. 1972; Bremer 1976; Roy 1996). The double-layered virus particle consists of a core particle formed by major structural proteins VP3 and VP7 (Grimes et al. 1998), surrounded by a diffuse outer VP2/VP5 capsid layer (Hewat et al. 1992), and encloses the three minor structural proteins (VP1, VP4 and VP6) and the 10 dsRNA genome segments.

The core particle is assembled by layering VP7 trimers on a VP3 scaffold. The VP7 trimers are formed by the interaction of three VP7 monomers, each with a top domain (amino acids 121-249) in the form of a β-sheet, flanked by the two bottom domains (amino acids 1-120 and 250-349) (Basak et al. 1996). The top domains of these trimers then form the outer layer of the core, whereas the bottom domains interact with the underlying VP3 layer (Grimes et al. 1995). Although the trimeric VP7 top domains of AHSV and BTV are structurally very similar, they have different effects on the solubility of the proteins (Monastyrskaya et al. 1997). AHSV VP7 is hydrophobic and insoluble (Roy et al. 1991; Basak et al. 1996) and in addition to being incorporated into core particles, it also self-assembles into large, flat, hexagonal crystalline particles. The particles are observed in the cytoplasm of AHSV-infected mammalian and insect cells (Burroughs et al. 1994; Venter et al. 2014), or in cells where VP7 is expressed from a

recombinant baculovirus (Chuma et al. 1992). These crystalline particles, easily observable even under a light microscope, are unique to AHSV compared to other orbiviruses and are characteristic of AHSV infection. In contrast to AHSV VP7, BTV VP7 is highly soluble and forms soluble trimers that are distributed evenly throughout the cytoplasm (Oldfield et al. 1990; Monastyrskaya et al. 1997; Kar et al. 2007). The solubility of BTV VP7 has allowed for the crystal structure of the protein to be determined via X-ray crystallography, but the same is not possible for AHSV VP7 due to its highly insoluble nature (Grimes et al. 1995; Basak et al. 1996). Thus, alternative avenues need to be explored when investigating the assembly and particle formation of AHSV VP7.

This particle-forming ability of AHSV VP7 was recently shown to be independent of host cell trafficking, and seems to be driven by factors such as VP7 trimer aggregation which are inherent to the protein itself (Bekker et al. 2014). In general, protein aggregation, and the assembly of such aggregates into supramolecular structures, can have a large impact on cellular biology and aspects associated with disease (Wu & Shea 2011). None of these aspects have been considered in the case of AHSV, and the role (if any) of VP7 aggregation in the life cycle of the virus is unknown.

To address the question of which of the VP7 characteristics are important in determining its intracellular localisation and crystalline particle forming ability, we previously generated VP7 mutants. These modifications involved insertion of six amino acids in the VP7 top domain downstream of residues 144, 177 and 200 respectively, generating VP7-144, VP7-177 and VP7-200 (Rutkowska et al. 2011). These modifications influenced both VP7 solubility and trimer stability. Whereas wild-

type (WT) VP7 and VP7-200 display less than 10% solubility, this increased to 30% for VP7-177 and to more than 60% for VP7-144. The VP7-200 trimers were however the least stable of the three constructs. When the VP7-144 protein was subsequently used for the insertion of full length enhanced green fluorescent protein (eGFP) into site 144, the fluorescing VP7-144-eGFP trimers were shown by confocal microscopy to localise to a single large focus of fluorescence similar to WT VP7 (Bekker et al. 2014). This implied that relatively major modifications to the AHSV VP7 top domain could be tolerated without affecting trimerisation, or the ability of the trimers to interact and assemble into large multimeric particulate structures.

The aim of this study was to do a full assessment of how top domain modifications affect AHSV VP7 localisation, assembly and particle formation. To this end we constructed VP7-177-eGFP and VP7-200-eGFP, and then compared the VP7 proteins containing minor top domain modification (VP7-144, VP7-177, VP7-200) and those containing the large eGFP insert (VP7-144-eGFP, VP7-177-eGFP, VP7-200-eGFP). The six different proteins were characterised by means of a microscopy-based approach to assess their particle-forming ability, and the VP7-eGFP fusion proteins analysed biochemically to determine their solubility, aggregation and fluorescence profiles. From the results it was concluded that the formation of the characteristic VP7 crystals in AHSV-infected cells is the result of a fine balance between VP7 solubility, trimer forming ability and trimer-trimer interactions.

MATERIALS AND METHODS

Construction of pFB-VP7-177-eGFP and pFB-VP7-200-eGFP and generation of recombinant baculoviruses for expression in insect cells

To generate VP7-eGFP fusion proteins, eGFP was inserted into the previously constructed AHSV-9 VP7 vectors pFB-VP7-177(P_1) and pFB-VP7-200(P_1) (Rutkowska et al. 2011). Primers flanked by HindIII (forward) and SalI (reverse) sequences were used to amplify the eGFP gene from a pGEM-Teasy-eGFP plasmid (supplied by Prof J. Theron, Department of Microbiology, University of Pretoria). Simultaneously, the pFB-VP7-177(P_1) and pFB-VP7-200(P_1) vectors were prepared for directional cloning by digestion with the restriction endonucleases HindIII and SalI. Standard cloning procedures were followed, and recombinant baculoviruses expressing VP7-177-eGFP and VP7-200-eGFP were generated using the Bac-to-Bac baculovirus expression system (Invitrogen) as described (Rutkowska et al. 2011). Pure viral stocks were prepared using standard procedures, and the titres determined by plaque assay in Sf9 cells.

Viruses and cells

Spodoptera frugiperda (Sf9) cells were cultured and maintained in suspension cultures as described (Rutkowska et al. 2011). Plaque-purified recombinant baculoviruses expressing WT AHSV-9 VP7, the modified AHSV-9 VP7 proteins VP7-144, VP7-177 and VP7-200, and VP7-144-eGFP were available at the start of this investigation (Maree et al. 1998; Rutkowska et al. 2011; Bekker et al. 2014). Sf9 cells were routinely infected with recombinant baculoviruses at a multiplicity of infection of 5.

Immunofluorescence microscopy

Sf9 cells seeded onto sterile coverslips were infected with recombinant baculoviruses and processed at 48 hours post infection (hpi). For direct immunofluorescence of constructs expressing eGFP, cells were rinsed once with phosphate buffered saline (PBS), followed by fixation in ice cold 50% methanol/50% acetone for 2-3 min. Nuclei were stained with 4',6-diamidino-2-phenylindole [DAPI, Roche Applied Science, 10 µg/µl in 1% blocking solution (1% milk powder in PBS)] for 10 min. Cells were rinsed and coverslips mounted onto glass slides using VECTASHIELD Mounting Medium (Vector Laboratories). For indirect immunofluorescence, cells were rinsed twice with PBS followed by 50% methanol/50% acetone fixation for 2-3 min. Cells were rinsed and incubated in 5% blocking solution (5% milk powder in PBS) for 30-60 min. Primary antibody labelling was done overnight at 4°C with a guinea-pig anti-VP7 antibody (Rutkowska et al. 2011) diluted 1:100. Cells were washed three times in wash buffer (0.05% Tween-20 in PBS) followed by secondary labelling for 1 hour at room temperature using anti-guinea pig IgG TRITC conjugate (Sigma Aldrich) diluted 1:250. Cells were washed before nuclear staining with DAPI, and coverslips were mounted onto glass slides as above. All slides were viewed, and channels collected sequentially, using a Zeiss LSM 510 Meta confocal scanning laser microscope and the images were obtained using the Zeiss LSM Image Browser Version 4.2.0.121. Colocalisation analyses were done on the Zeiss LSM files by using Image J software (Version 1.43m, http://rsb.info.nih.gov/ij).

High-pressure freezing and freeze substitution (HPF-FS)

Baculovirus-infected Sf9 cells were gently dislodged from the flask at 48 hpi by scraping, and a cell pellet obtained by low speed centrifugation at 1 000 rpm for 5 min.

A 0.5 µl sample of the cell pellet was transferred onto a dry Leica membrane specimen carrier coated with L-α-Phosphatidylcholine (10 mg ml^{-1}, Sigma Aldrich) and frozen to -196˚C following pressurisation to 2 000 bar within 10 milliseconds in a Leica EMPACT2 high-pressure freezing (HPF) apparatus (Studer et al. 2001). Following HPF, freeze substitution (FS) was done in a Leica AFS2 FS apparatus in the presence of a FS mixture of ethanol containing 1% distilled water. The temperature was increased logarithmically from -90°C to 0°C over a period of 72 hours, after which membrane carriers were removed from the FS machine and .washed three times with 100% ethanol. Cell samples were then transferred to Eppendorf tubes and submerged in 100% ethanol prior to resin embedding.

Resin embedding and transmission electron microscopy (TEM)

In preparation for immunogold labelling and TEM, resin embedding was done using LR White (SPI Supplies). The 100% ethanol present after HPF-FS was gradually replaced with clean LR White resin. Polymerisation of the cell sample in the LR White resin was at 65˚C for 48 hours, followed by ultrathin (100 nm) sectioning using a Reichert Jung Ultracut E microtome and a diamond knife (DiATOME, US). Staining was in 1% uranyl acetate for 10 min and Reynold's lead citrate for 3 min (Reynolds 1963), followed by visualisation on a JEOL JEM-2100F field emission transmission electron microscope.

Immunogold labelling for TEM

Samples were incubated for 1.5-2 hours in blocking buffer (0.1 M potassium phosphate buffer (pH 7.2), 5% FCS, 0.05% Tween-20). The potassium phosphate buffer was used instead of PBS to minimise the presence of salt crystals. Primary

antibody labelling was for 1.5-2 hours with either the guinea pig anti-VP7 (described above) or anti-GFP (Sigma Aldrich, G1544) antibodies diluted in blocking buffer (1:100 and 1:500 respectively) and grids washed twice for 2 min with blocking buffer and twice for 2 min with potassium phosphate buffer. Secondary antibody labelling was for 1 hour with either anti-guinea pig or anti-rabbit 10 nm Colloidal Gold antibody (SPI Supplies) diluted 1:30 in blocking buffer, followed by another set of wash steps. Once dry, grids were stored for future TEM viewing. Measurement of the dimensions of WT VP7, VP7-177 and VP7-200 particles was done using iTEM software (Olympus Software Imaging Solutions iTEM TEM imaging platform).

Sucrose density sedimentation analyses

Infected Sf9 cells were harvested at 24, 30, 38 or 48 hpi by centrifugation at 2 000 revolutions per minute (rpm) for 5 min, resuspended in 1 ml Lysis buffer [0.01 M STE (10 mM Tris, 50 mM EDTA, 10 mM NaCl, pH 7.4), 0.5% Nonidet P-40 (NP-40, Boehringer Mannheim)] followed by 30 min incubation on ice and then dounce homogenisation. Where indicated, lysates were treated to a final concentration of 1 M L-arginine. Lysates were loaded onto 30-80% (w/v in PBS) discontinuous sucrose density gradients and centrifuged in a Beckman Coulter Optima^{TM} L-80 Ultracentifuge (SW55Ti rotor) at 30 000 rpm for 21 hours at 4°C. Fractions were collected from the bottom of each tube and the pellet was resuspended in PBS. In the VP7-eGFP trimerisation assay the lysates were centrifuged on 10-40% (w/v in PBS) sucrose gradients for 21 hours at 50 000 rpm in a SW55Ti rotor to provide optimum separation of trimers and monomers.

VP7 protein analysis via SDS-PAGE and immunoblotting

The protein content of the fractions and pellets was analysed by 12% SDS-PAGE and stained with Coomassie Brilliant Blue. For immunoblot analyses the proteins were transferred to a Hybond C extra nitrocellulose membrane (Amersham Biosciences) via standard blotting procedures. Membranes were incubated with the anti-GFP antibody described above, diluted 1:4 000, and detected using peroxidase-conjugated Protein A (Calbiochem) diluted 1:10 000.

The relative amount of VP7-eGFP protein was calculated from immunoblots by scanning the VP7-eGFP bands in each fraction using the EZQuant software package (EZQuant Ltd.). The relative distribution of the proteins on the gradients was then determined from the densitometer value of each gradient fraction expressed as a percentage of the combined total of all the fractions. The fluorescence emitted by the fractions was measured by a Fluoroskan Ascent FL Fluorometer (Thermo Labsytems).

RESULTS

In order to evaluate the effect of VP7 top domain modifications on the self-assembly ability of the protein, and the nature of the resulting particles, we utilised seven different recombinant baculoviruses expressing WT VP7, VP7-144, VP7-177, VP7-200 (Rutkowska et al. 2011), VP7-144-eGFP (Bekker et al. 2014), VP7-177-eGFP and VP7-200-eGFP (constructed as part of this study, see below). Fig. 1 gives a schematic representation of these proteins, indicating the relative positions and detail of the insertions.

Intracellular distribution and particle formation of AHSV VP7 proteins containing minor top domain modifications

The effect of the three small peptide insertions on the intracellular localisation and particle formation of AHSV VP7 was first investigated, using a dual confocal and transmission electron microscopy approach. Sf9 cells expressing WT VP7, or the modified VP7-144, VP7-177 or VP7-200 proteins were harvested at 48 hours post infection (hpi) and chemically fixed for immunofluorescence, or preserved by high pressure freezing and freeze-substitution (HFP-FS) for transmission electron microscopy (TEM). A primary anti-VP7 antibody was used in conjunction with TRITC- or gold-conjugated secondary antibodies for immunofluorescence and immunogold labelling respectively, with uninfected and wild type baculovirus infected cells displaying little to no background labelling (not shown).

Confocal microscopy revealed the presence of one, and occasionally two or three, large (2 - 5 µm) crystalline particles in the cytoplasm of cells expressing WT AHSV VP7 (Fig. 2A). Three-dimensional rendering of Z-stack analysis (Supplementary Fig. 1) confirmed that these particles were flat structures which, depending on the focal plane and cellular orientation, were observed as hexagonal-shaped particles when viewed from one angle (Fig. 2B), or were visualised as long rod-like structures when viewed at a 90° rotation (Fig. 2C). TEM analysis of ultrathin sections of cells also showed rectangular crystalline structures of varying sizes, which gave strong positive labelling with anti-VP7 antibodies (Fig. 2D). These represent sections through the flat hexagonal crystals, and display the same ultrastructure as described for the VP7 crystals formed in AHSV-infected cells (Venter et al. 2014).

Confocal immunofluorescence microscopy indicated that the modified VP7-144 (Fig. 2E, F), VP7-177 (Fig. 2I, J) and VP7-200 (Fig. 2M, N) proteins were, as in the case of WT VP7, also localised to one or two specific sites within the cell. However the particulate structures assembled at the site of localisation were distinctly different from each other and from WT VP7. The higher resolution of the TEM showed that in cells expressing VP7-144 the VP7-specific antibody-labelled structures had the appearance of either spindle-like fibres (Fig. 2G), or smaller loosely associated granular structures (Fig. 2H). These spindles or granules would represent thin sections through the fluorescing rosette-like aggregates and foci respectively (Fig. 2E, F) observed via the confocal microscope. The aggregates assembled from VP7-177 (Fig. 2K, L) and VP7-200 (Fig. 2O, P) appeared to be more rigid in structure than those of VP7-144, and more closely resembled the solid WT VP7 crystals (Fig. 2D). However rather than forming a single crystalline structure, the VP7-177 and VP7-200 aggregates appeared rosette-like, with multiple rod-like particles in the same region. The interpretation from the 3D-rendering of the confocal images (not shown) was that these structures were the result of multiple flat sheets of aggregated VP7, stacked in close proximity to each other. Measurement of the dimensions of the particles using iTEM software showed that the average thickness of the VP7 structures was 244 nm for WT VP7 (n = 23), 219 nm for VP7-177 (n = 56) and 101 nm for VP7-200 (n = 75).

From this we concluded that minor modifications to the VP7 top domain did not influence the ability of VP7 to self-assemble into one or a few large particles within the cell's cytoplasm, but that these small insertions did affect the nature of the particles to a lesser or greater extent.

Intracellular localisation and ultrastructure of the VP7-eGFP constructs

It was previously shown that the insertion of eGFP into the site 144 resulted in VP7-144-eGFP being localised, similar to WT AHSV VP7, to a single large focus in the cell (Bekker et al. 2014). We additionally prepared constructs with eGFP inserted into sites 177 and 200. The VP7-144-eGFP, VP7-177-eGFP and VP7-200-eGFP proteins were expressed in Sf9 cells, and the subcellular localisation and ultrastructure of the VP7 fusion proteins comparatively visualised via direct immunofluorescence imaging by confocal microscopy or by transmission electron microscopy.

VP7-144-eGFP formed large cytoplasmic foci of strong fluorescence (Fig. 3A, B). Small aggregates were observed early after infection (24 or 30 hpi, not shown) but these smaller aggregates were almost completely absent in cells by 48 hpi when large foci had formed. From Z-stack analyses and 3D reconstructions (not shown) it was concluded that these fluorescent foci were irregular in shape, and mostly in the form of a flattened sphere. TEM and immunogold labelling showed that there were both smaller loosely arranged aggregates (Fig. 3C) and larger, more rigid irregularly shaped electron-dense structures (Fig. 3D) in the cytoplasm of infected cells that were composed of the VP7-144-eGFP protein.

Cells expressing either VP7-177-eGFP (Fig. 3E, F) or VP7-200-eGFP (Fig. 3I, J) displayed multiple foci of strong fluorescence, which never converged into a single large fluorescing unit. The VP7-177-eGFP foci had a spherical appearance, while the VP7-200-eGFP foci were flat and disc-shaped. Ultrastructurally, both the VP7-177-eGFP and VP7-200-eGFP foci appeared to be composed of multiple smaller protein

aggregates of no clearly defined shape (Fig. 3G, K, L), with VP7-177-eGFP occasionally displaying a more densely packed oval-shaped format (Fig. 3H).

Where in the case of VP7-144-eGFP the initial smaller foci coalesced into one large particulate structure, this process appeared to be blocked at some level for VP7-177-eGFP and VP7-200-eGFP, resulting in multiple small foci being maintained throughout the cytoplasm. This differential trafficking and/or assembly of the three VP7-eGFP fusion proteins could relate to the ability of the proteins to fold or trimerise correctly. The images observed through the confocal microscope would represent only fusion proteins displaying a correctly folded and therefore fluorescing eGFP component. The electron micrographs however act as no indicator of protein conformation, and the gold-labelled VP7-specific subcellular structures may well also have been assembled from misfolded non-fluorescing proteins.

The solubility and trimerisation profile of VP7-eGFP fusion proteins

In an attempt to elucidate the reason behind the differential intracellular coalescing behaviour of the VP7-eGFP fusion proteins, a number of additional experiments were performed to assess the solubility, fluorescence and trimerisation ability of the three constructs. Firstly, the solubility profiles of the proteins were investigated via sucrose gradient sedimentation. Cellular lysates of Sf9 cells containing baculovirus expressed VP7-144-eGFP, VP7-177-eGFP or VP7-200-eGFP proteins were harvested at 48 hpi, treated with L-arginine to prevent protein aggregation (Tsumoto et al. 2005) and the soluble and particulate forms of the proteins separated by centrifugation through 30-80% w/v sucrose gradients. Gradient fractions were collected, and the protein content of each fraction analysed by immunoblotting using eGFP antibodies. Quantification of

the blots was done to provide an estimation of the relative amount of VP7-eGFP fusion protein in each gradient fraction (Fig. 4A). All experiments were repeated at least three times. Based on these quantifications, the total amount of the VP7-eGFP protein expressed was approximately the same for each of the three constructs. Subsequently the fluorescence value of each of the fractions was measured and plotted (Fig. 4B), this represented the proportion of fluorescing and therefore correctly folded VP7-eGFP fusion protein per fraction. The bulk of the fluorescing proteins sedimented in the upper soluble fractions of the gradient, indicated by a double arrow (Fig. 4B, fractions 16-25), whereas the aggregated fraction of the total VP7-eGFP proteins expressed sedimented in the lower region of the gradients (Fig. 4A, fractions 3-14). In all three constructs, but especially so in the case of VP7-177-eGFP and VP7-200-eGFP, a large proportion of the expressed protein was non-fluorescing and therefore presumed to be misfolded with respect to the eGFP insert.

The total protein profiles (Fig. 4A) would represent a combination of both correctly folded (fluorescing) and misfolded (non-fluorescing) proteins. Based on the total amount of protein synthesised, VP7-144-eGFP was found to be the most soluble of the proteins with a soluble fraction of about 36%, compared to approximately 17% for both VP7-177-eGFP and VP7-200-eGFP. As the yield of fluorescent VP7-144-eGFP protein was at least three times that of either fluorescent VP7-177-eGFP or VP7-200-eGFP (Fig. 4B), it indicated that insertion of eGFP into site 144 ensured a more optimised environment for correct folding. In all three VP7-eGFP fusion proteins the bulk of the fluorescing VP7-eGFP protein was not associated with stable particulate structures.

The trimer stability of the three VP7-eGFP constructs was determined by sucrose sedimentation analysis on 10-40% w/v sucrose gradients in the presence of bovine serum albumin (66 kDa), L-lactate dehydrogenase (140 kDa) and catalase (250 kDa) markers. The distribution of the VP7-eGFP proteins on the gradient was assessed from fluorescence readings of fractions, whereas the positions of the marker proteins were determined by SDS-PAGE of the protein subunits (not shown). Visualisation of the gradients under ultraviolet light before fractionation (Fig. 5A) clearly indicated the presence of a single fluorescing band for VP7-144-eGFP and VP7-177-eGFP, in contrast to two bands with different sedimentation rates for VP7-200-eGFP. Subsequent fractionation of the gradients and comparison to the marker proteins (Fig. 5B) showed that the slower sedimenting fractions (10-13) of VP7-200-eGFP corresponded in molecular mass to the 66 kDa albumin marker, indicating that this was a VP7-eGFP monomer, whereas the faster sedimenting fluorescing fractions (3-7) of VP7-200-eGFP, and the fluorescing peak for VP7-144-eGFP and VP7-177-eGFP, sedimented in a position just less than 200 kDa, which would correspond to the molecular mass of a VP7-eGFP trimer.

Synthesis of VP7-eGFP fusion proteins at different times after infection

To investigate how the ratio of correctly folded versus misfolded protein was affected by the level to which the proteins are expressed early in the baculovirus expression cycle, cell lysates containing VP7-144-eGFP and VP7-200-eGFP proteins were prepared at 24, 30 and 38 hpi and analysed by sucrose gradient sedimentation both before and after L-arginine treatment. The two fusion proteins characterised represented two constructs with distinct differences in trimer stability and solubility.

Total protein sedimentation profiles were obtained from immunoblots, and compared to the corresponding fluorescence profiles (Fig. 6A).

The results indicated that the bulk of the fluorescing VP7-144-eGFP proteins synthesised between 24 and 38 hpi aggregated to form larger molecular weight complexes that could be dissociated into soluble trimers by L-arginine treatment. In contrast there was little evidence of aggregation of fluorescing VP7-200-eGFP into larger complexes, and the profile of either the fluorescing or misfolded/non-fluorescing VP7-200-eGFP proteins was not significantly affected by L-arginine treatment. The difference between the two fusion proteins was quantified by calculating the ratio of the total amount of fluorescing protein in a gradient versus the total amount of protein expressed. These values were normalised to a value of 100% at 24 hpi and then calculated for each of the gradients in Fig. 6A. The result (Fig. 6B) shows that whereas this ratio seemed to increase or stay largely the same in the case of VP7-144-eGFP, the ratio immediately declined in VP7-200-eGFP and at 38 hpi it was reduced to less than 10% of its original value at 24 hpi. This indicated that from after 30 hpi the majority of newly synthesised VP7-200-eGFP was cold and presumed to be misfolded.

Fate of misfolded VP7-eGFP proteins

To assess whether the non-fluorescing misfolded VP7-eGFP fusion proteins showed a different distribution in the cell compared to their correctly folded fluorescing counterparts, the proteins were expressed in Sf9 cells, fixed at 48 hpi, immunolabelled with an anti-VP7 antibody and a TRITC-conjugated secondary antibody and imaged at two different wavelengths. Under these conditions correctly folded and fluorescing proteins would show both green eGFP auto-fluorescence as well as a red signal

resulting from the anti-VP7 labelling. Misfolded and non-fluorescing protein on the other hand would be detected by a red signal only, with the absence of any green fluorescence.

The results in Fig. 7 show that for all three VP7-eGFP constructs the green auto-fluorescence and red antibody recognition signals colocalised. This was quantified using Image J software to determine the Manders' coefficient (Bolte & Cordelieres 2006). Manders' coefficients of 0.890 (n = 16), 0.872 (n = 25) and 0.911 (n = 16) were obtained for VP7-144-eGFP, VP7-177-eGFP and VP7-200-eGFP infected cells respectively, indicating a high level of colocalisation in all cases. These results suggested that the misfolded VP7-eGFP fusion proteins observed via sucrose gradient sedimentation analyses localised to the same position as the correctly folded fluorescing proteins.

DISCUSSION

Protein aggregation and the assembly of such aggregates into supramolecular structures has received a significant amount of attention in the literature because of its impact on cellular biology and toxicity and disease (Lorenzo & Yankner 1994; Bucciantini et al. 2002; Stefani 2004; Wu & Shea 2011; Amin et al. 2014; Roberts 2014). When AHSV VP7 is expressed in mammalian or insect cells, the protein trimers localise to one or two sites in the cell and assemble into large flat hexagonal crystalline particles (Burroughs et al. 1994; Venter et al. 2014) which have recently been shown to impede the formation of core-like particles (Maree et al. 2016). This characteristic is unique to AHSV, and presents a distinct difference between major capsid protein VP7 of AHSV and BTV (Monastyrskaya et al. 1997). The possible role of this

genetically conserved distinction is not known, and it remains unclear why the bulk of the VP7 synthesised within an infected cell is channelled into these particles.

The impact of AHSV VP7 trimer aggregation and particle assembly on virus replication and cellular biology has not been studied. As part of this larger question, it is important to understand how VP7 is localised to the particle crystallisation site, and what determines the particle morphology. Bekker et al. (2014) recently showed that the intracellular distribution and movement of AHSV VP7 to the sites of particle formation is not cell-type dependent, does not utilise cellular trafficking or degradation pathways, and is not influenced by the presence or absence of other AHSV proteins. It is therefore the result of inherent properties of AHSV VP7, even though the factors that determine these characteristics have not been identified. We sought to characterise some of these aspects through analysing selective site- and insert-specific modifications to the VP7 top domain that affected VP7 solubility, VP7 trimer stability, localisation and particle formation.

The data obtained indicated that small top domain peptide insertions which resulted in constructs which ranged in solubility from less than 10% (VP7-200) to 30% (VP7-177) and more than 60% (VP7-144) did not affect their intracellular distribution. Similar to WT VP7, all were localised to the one or two sites of assembly in the cytoplasm. VP7 solubility alone is therefore not the determining factor in the localisation of these proteins with minor top domain modifications. These minor modifications did however disrupt the stable layering of the trimers into the characteristic WT VP7 crystalline particles. The most striking difference was with respect to the most soluble of these constructs, VP7-144, which formed spindle-like fibres or loosely associated granular

particles that did not resemble the hexagonal VP7 structure. Sucrose gradient sedimentation analysis of cellular lysates containing VP7-144 (results not shown) confirmed that these aggregates were unstable and could be fully converted to a soluble protein by treatment with L-arginine. The VP7-177 and VP7-200 constructs formed particles that more closely resembled those of WT VP7, but instead of the solid flat hexagonal WT VP7 particles of about 244 nm thick, VP7-177 and VP7-200 formed L-arginine-stable, multi-layered rosette-like structures composed of sheets with a thickness of on average 219 and 101 nm respectively.

The insertion of eGFP into the top domain resulted in distinct differences with respect to the trafficking and aggregation of the three VP7-eGFP fusion proteins. Whereas the VP7-144-eGFP trimers accumulated at one or two large foci in the cytoplasm, their VP7-177-eGFP and VP7-200-eGFP equivalents formed multiple smaller foci throughout the cell. The aggregates of the eGFP-containing VP7 proteins were electron dense particulate structures, lacking any well-defined crystalline shape. It has been shown that the attachment of a fluorescent eGFP tag to a protein can have an effect on its cellular distribution (Heymann et al. 2015) whereas our results indicated that the site of eGFP insertion can also play a role. From our further results we concluded that the observed differences in localisation may be linked to differences in the proportion of misfolded versus correctly folded VP7-eGFP fusions proteins. Between 24 and 38 hpi the fraction of fluorescing correctly folded VP7-200-eGFP declined to less than 10% of its value at 24 hpi, in stark contrast to VP7-144-eGFP where no reduction was observed in the same period. This could be explained by space constraints with respect to eGFP folding. The three 200 sites in the VP7 trimer are clustered in close proximity to one another at the centre of the trimer, whereas the

144 sites in the VP7 trimer are located far apart on the outer perimeter (Rutkowska et al. 2011).

To explore how protein misfolding could affect localisation we addressed the question of whether or not misfolded proteins were localised differently from their correctly folded fluorescing counterparts. Confocal analyses of their distribution and a calculation of the respective Manders' coefficients (Bolte & Cordelieres 2006) indicated that in all cases the non-fluorescing misfolded VP7-eGFP fusion proteins localised to the same positions or foci in the cell as the correctly folded fluorescing proteins. Earlier results (Bekker et al. 2014) have shown that the localisation of VP7-144-eGFP is facilitated by VP7 aggregation and the formation initially of small foci, which eventually coalesce at one or two large foci. In the case of VP7-177-eGFP and VP7-200-eGFP the localisation of both fluorescing and misfolded proteins appears to be blocked at the level of the smaller foci. Such blockage will happen at the stage when the proteins self-assemble into large insoluble protein complexes. The threshold at which this occurs is linked to solubility (Dobson 2004). Misfolded VP7-177-eGFP and VP7-200-eGFP proteins are likely to be characterised by a large reduction in solubility and this aggregation threshold is reached more easily, and at the concentration level at the smaller foci, than that of the more soluble and more correctly folded VP7-144-eGFP constructs. The localisation of VP7-177-eGFP and VP7-200-eGFP was not affected by the large differences in the trimer stability of these proteins. It is possible that within the environment of the cell, the VP7-200-eGFP trimers are sufficiently stable to allow trafficking through trimer-trimer interactions similar to that of VP7-177-eGFP.

In the mature AHSV virion the VP7 trimers form the outer core layer, with the base of the trimer (bottom domain) interacting with VP3 in the inner core, and the top domain in contact with the outer capsid proteins VP2 and VP5. One would therefore not expect the top domain to necessarily be involved in trimer-trimer interactions. We were interested in why the protein also localises to discreet foci in a cell without interaction of any other viral proteins, and what triggers AHSV VP7 particle formation. None of the modifications we introduced prevented trafficking, however modifications that resulted in VP7-eGFP fusions with a misfolded eGFP insert, appeared to block trafficking at the stage where small foci coalesce to one or more large foci. The nature of the top domain however impacted on the ultrastructure of the particles that were assembled at these foci, be they one or multiple.

CONCLUSION

Using a dual confocal and transmission electron microscopy approach supplemented with biochemical data we here investigated the intracellular localisation, aggregation and particle formation of AHSV VP7 in the crystal. Minor modifications to the top domain did not interfere with trafficking of the protein to a single point of aggregation in the cytoplasm, but did affect the stable layering of trimer sheets into one solid crystalline particle. The effect of inserting the large eGFP protein into the top domain depended on the site used. The insertion of eGFP into sites 177 and 200 blocked coalescence of all fluorescing proteins into a single aggregate, and resulted in multiple cytoplasmic foci of the VP7-eGFP fusion proteins. Based on the integration of the biochemical and microscopy data, this was attributed to the accumulation of misfolded and insoluble fusion proteins that interfered with further trimer-trimer interactions.

All our results support the hypothesis that trafficking of VP7 is driven by trimer-trimer interactions, and the fact that this included misfolded proteins indicates something about the prominence of this interaction. What still remains unknown is what drives VP7 trimer-trimer interactions, and the relevance of this trimer-trimer interaction in the assembly of AHSV particles. This will be addressed in future by identification of VP7 mutations that abolish trimerisation, and assessment of their effect in the context of the viral life cycle by using a reverse genetics approach.

ACKNOWLEDGEMENTS

This work was supported by BioPad Bric Grant BP050 and the Poliomyelitis Research Foundation, South Africa, Grant 10/12. Postgraduate support was received from the Poliomyelitis Research Foundation, South Africa, Grant 11/62, the National Research Foundation, South Africa and the University of Pretoria, South Africa. The funding bodies had no involvement in the study design, collection, analysis and interpretation of data, the writing of the manuscript, nor the decision to submit the work as an article for publication. We thank Mr Flip Wege for technical support with cell culture. We also thank the Laboratory for Microscopy and Microanalysis at the University of Pretoria, South Africa, especially Mr Alan Hall and Ms Soné Hendriks for their assistance with confocal microscopy, as well as Mr Chris van der Merwe and Ms Antoinette Buys for their assistance with transmission electron microscopy.

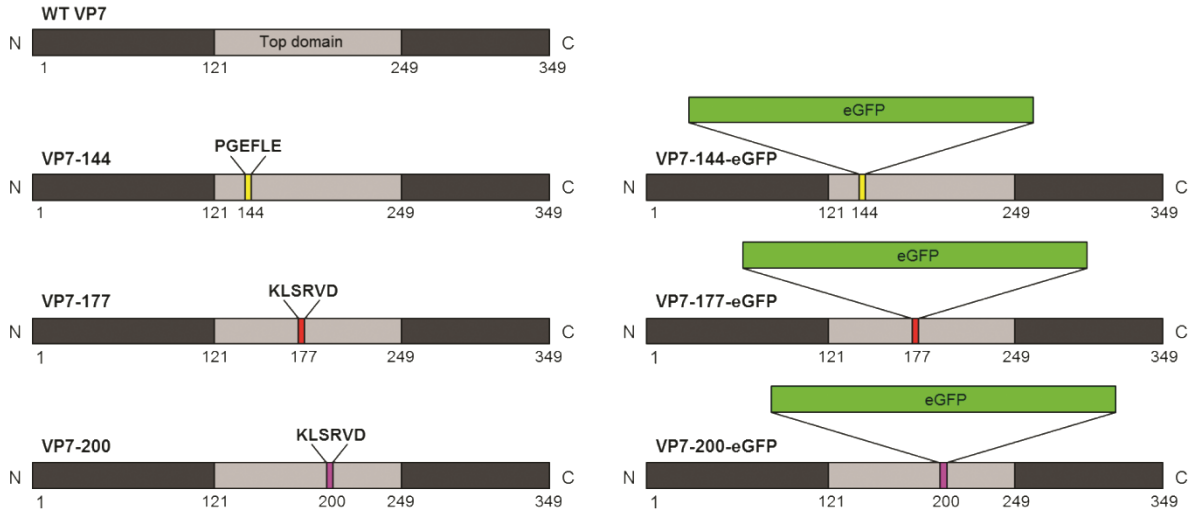

Fig. 1. Schematic representation of the AHSV VP7 constructs used in this study. The top domain is indicated in grey and the bottom domain in black. The top domain sites targeted for minor top domain modifications were sites 144, 177 (red) and 200 (magenta), with the amino acid insertions indicated above each protein at the insertion site. This yielded the vector proteins VP7-144, VP7-177 and VP7-200. eGFP (green) was inserted into each of the three sites yielding three VP7-eGFP fusion proteins. Figure adapted from Rutkowska et al. (2011).

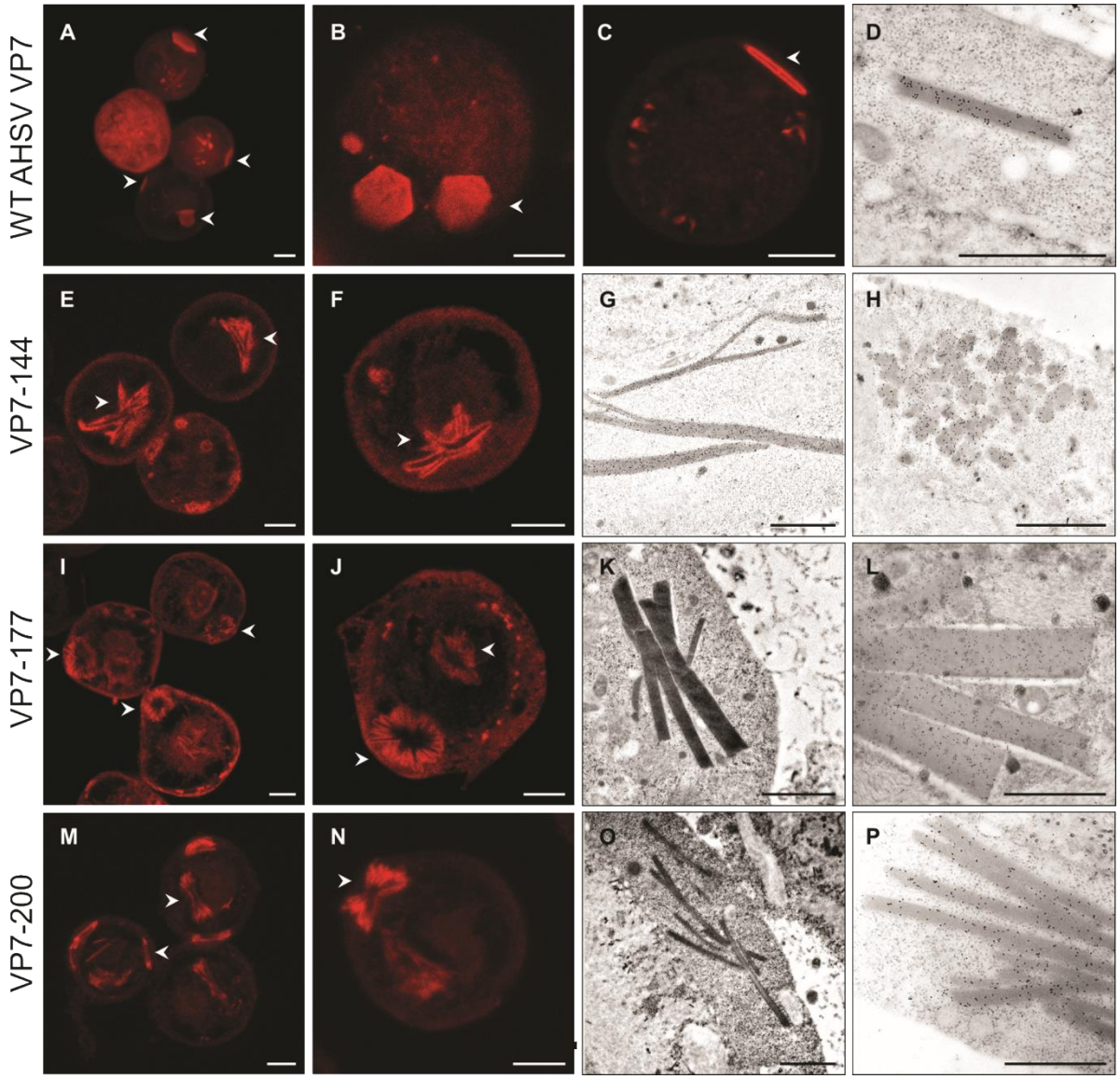

Fig. 2. Immunofluorescence and TEM images of Sf9 cells expressing WT AHSV VP7, VP7-144, VP7-177 or VP7-200. At 48 hpi, cells were either fixed and prepared for indirect immunofluorescence (A-C, E, F, I, J, M, N), or preserved by HPF-FS for TEM (D, G, H, K, L, O, P). VP7 protein was detected using guinea pig anti-VP7 primary and TRITC-conjugated fluorescing secondary antibodies (red). Immunogold labelling was done using guinea pig anti-VP7 primary and anti-guinea pig 10 nm Colloidal Gold secondary antibodies. The arrowheads indicate the hexagonal (A, B) or rod-like crystalline particles (when viewed from a 90° angle, A, C) formed by WT AHSV VP7

as well as the particles formed by VP7-144, VP7-177 or VP7-200 (E, F, I, J, M, O). Bars, 5 µm (A-C, E, F, I, J, M, N); 1 µm (D, G, H, K, L, O, P).

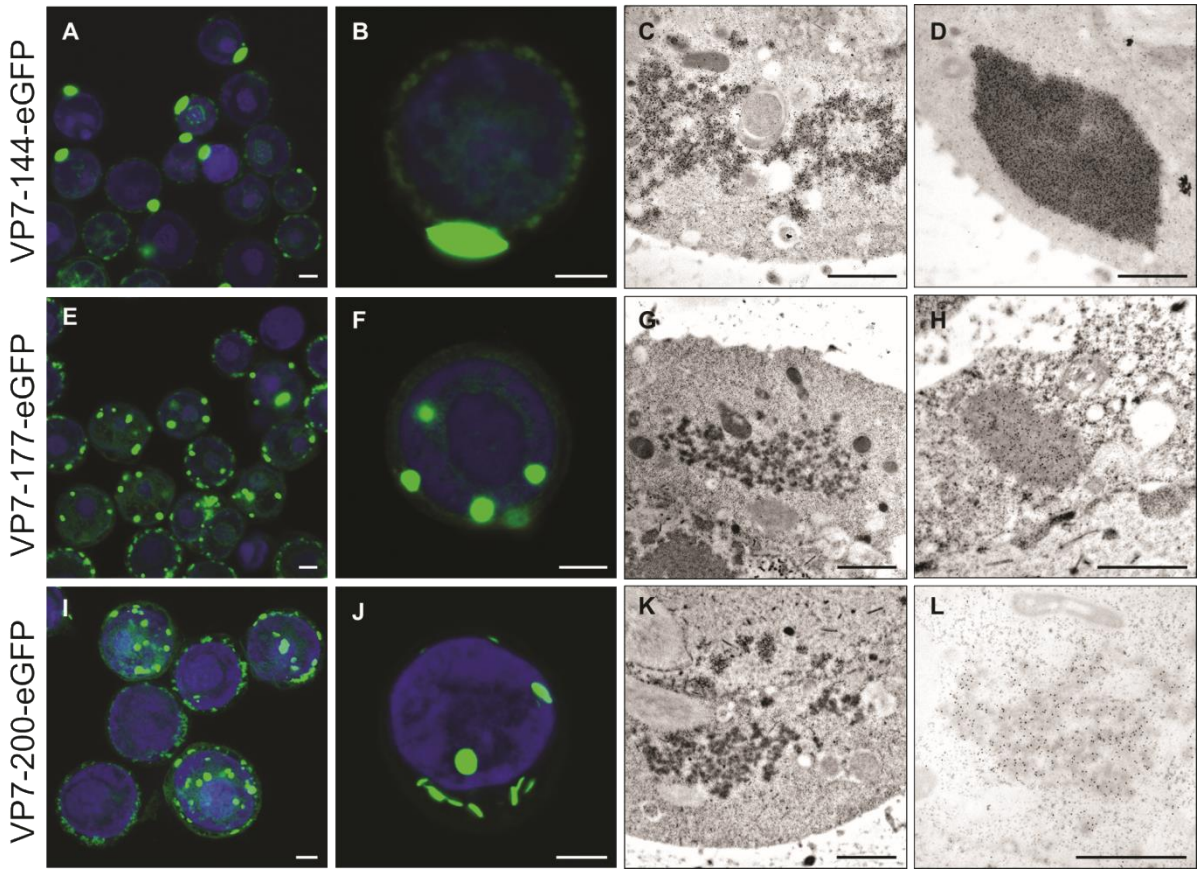

Fig. 3. Immunofluorescence and TEM images of Sf9 cells expressing VP7-144-eGFP, VP7-177-eGFP or VP7-200-eGFP. At 48 hpi, cells were either fixed and prepared for direct immunofluorescence (A, B, E, F, I, J), or preserved by HPF-FS for TEM (C, D, G, H, K, L). VP7-eGFP fusion proteins were visualised based on green auto-fluorescence and nuclei were stained with DAPI (blue). Immunogold labelling was done using anti-GFP primary and anti-rabbit 10 nm Colloidal Gold secondary antibodies (C, D, H, L). Bars, 5 µm (A, B, E, F, I, J); 1 µm (C, D, G, H, K, L).

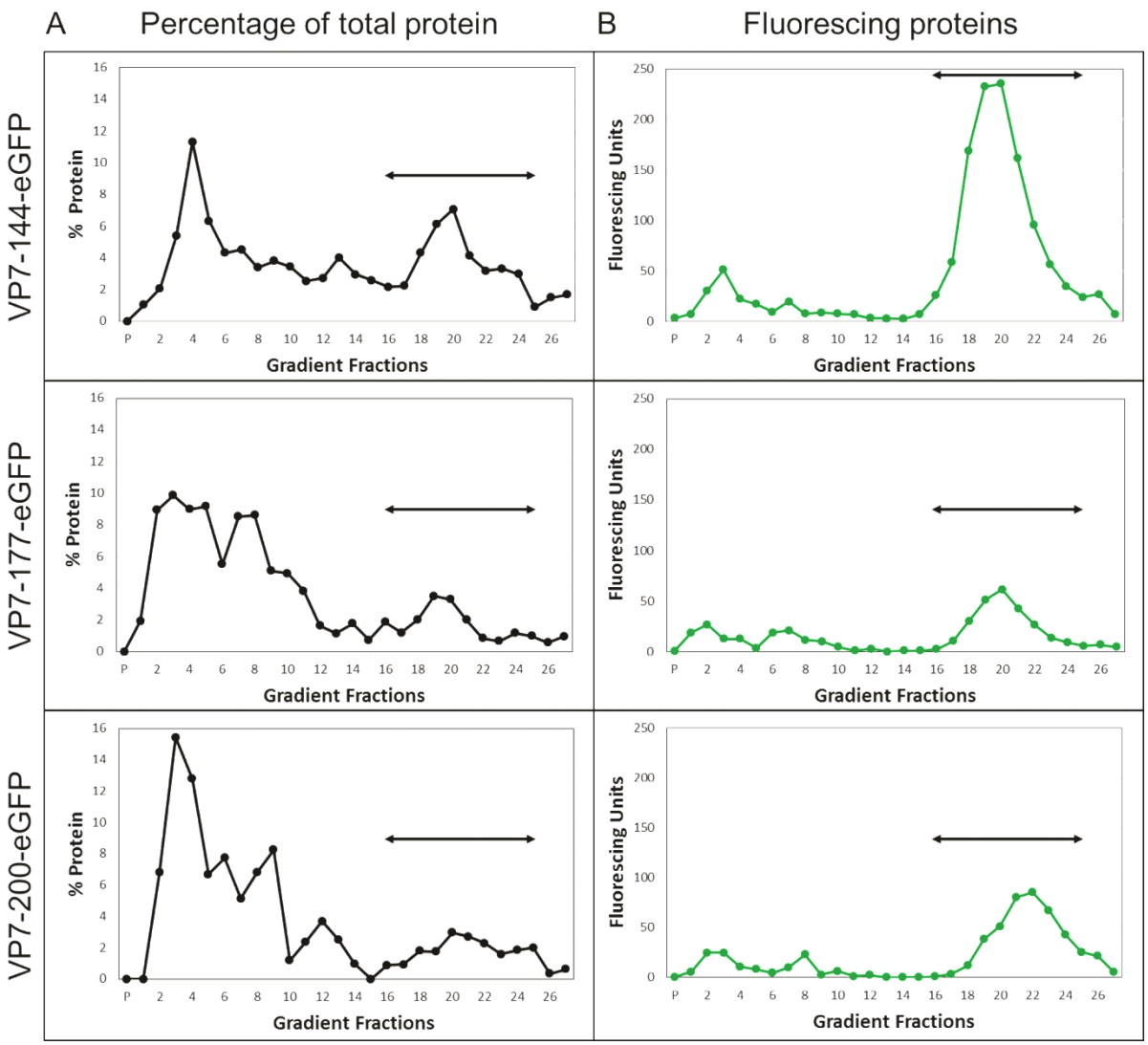

Fig. 4. Sucrose gradient sedimentation analysis of L-arginine treated cellular lysates containing VP7-144-eGFP, VP7-177-eGFP and VP7-200-eGFP proteins harvested at 48 hpi. Gradient fractions were analysed by immunoblotting with GFP antibodies. The relative amounts of the VP7-eGFP proteins were determined from scanned immunoblots and the densitometer value of each gradient fraction is shown as a percentage of the combined densitometer value of all the gradient fractions (A). The fluorescence emission was measured for each of the gradient fractions (B). The double-sided arrow indicates the fractions containing soluble proteins.

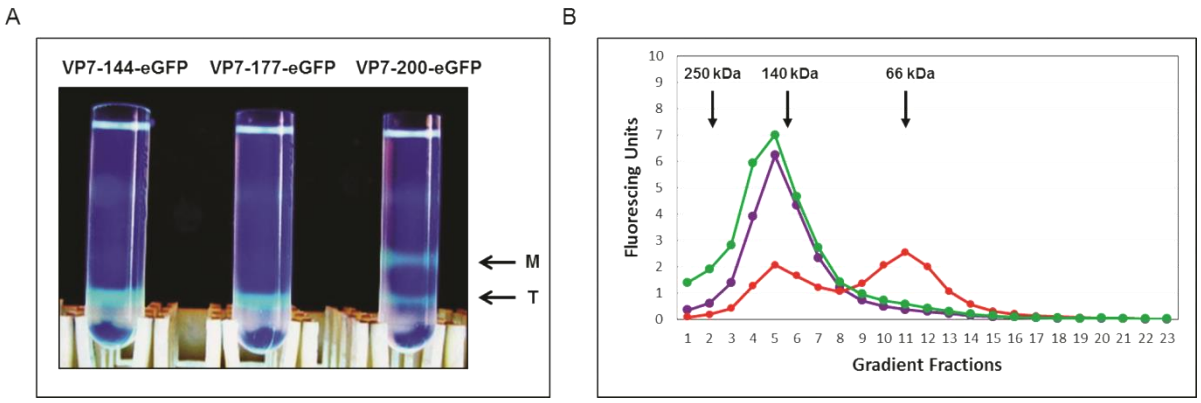

Fig. 5. Sedimentation analysis of VP7-144-eGFP, VP7-177-eGFP and VP7-200-eGFP. Exposure of the sucrose gradients to ultraviolet light allowed identification of monomeric (M) and trimeric (T) versions of the fusion proteins at different positions in the centrifuge tubes (A). After fractionation of the gradients the sedimentation profile of soluble fluorescing VP7-144-eGFP (green), VP7-177-eGFP (purple) and VP7-200-eGFP (red) could be compared to those of known soluble marker proteins bovine serum albumin (66 kDa), L-lactate dehydrogenase (140 kDa) and catalase (250 kDa) (B).

A

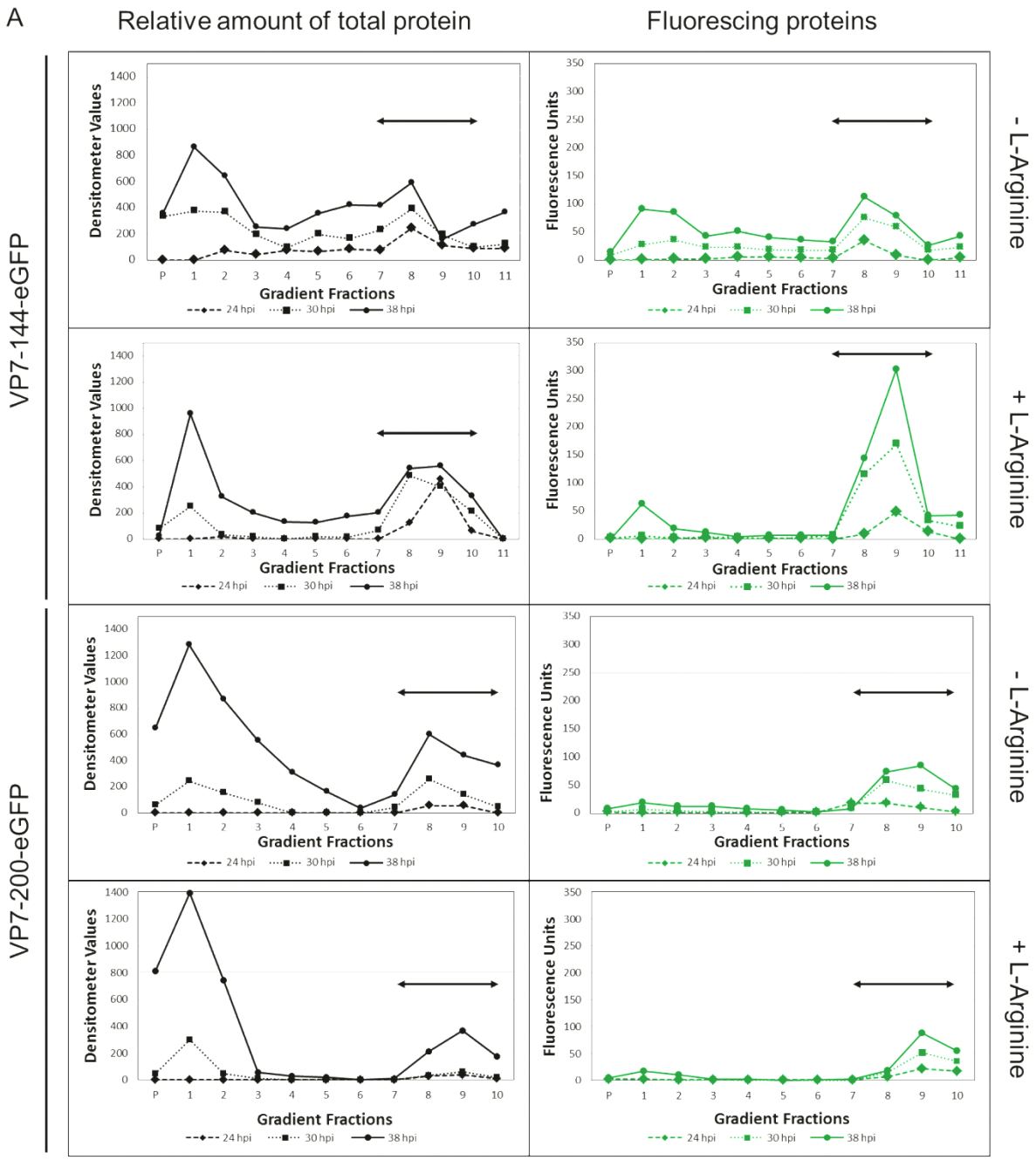

B

% Change in the ratio of fluorescing versus total VP7-eGFP protein expressed

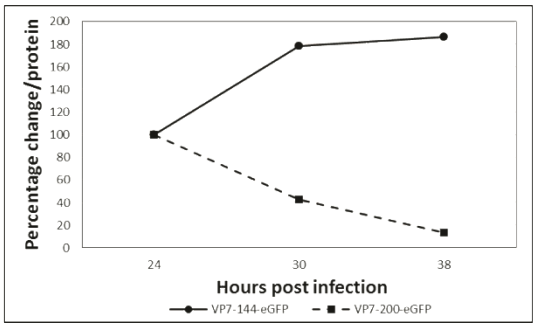

Fig. 6. (A) Sedimentation analysis of baculovirus expressed VP7-144-eGFP and VP7-200-eGFP proteins at 24, 30 and 38 hpi in cellular lysates with and without L-arginine treatment. Gradient fractions were subjected to immunoblots with an anti-GFP antibody and scanned to determine the relative densitometer values for the VP7-eGFP fusion proteins (A) and compared that of the relative distribution of the fluorescing proteins (B). The double-sided arrow indicates the soluble fraction of the gradient. The ratio of correctly folded eGFP fusion protein versus the total amount of accumulated fusion protein at each time point (B) was calculated from the percentage of total fluorescing protein as a fraction of the total accumulated VP7-eGFP protein. All values were normalised to a value of 100% at 24 hpi to reflect the change in this ratio.

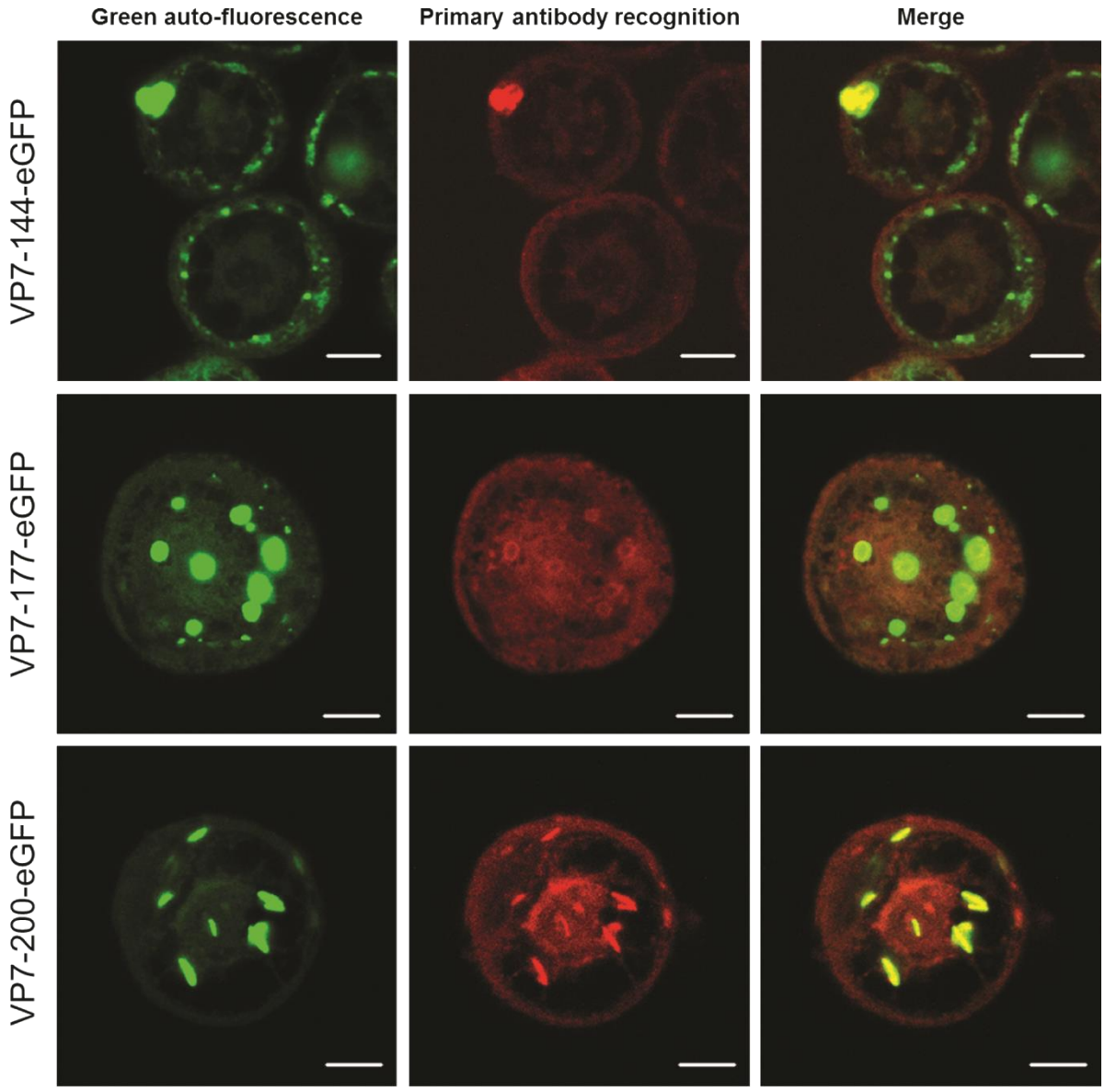

Fig. 7. Immunofluorescence images of Sf9 cells infected with recombinant baculoviruses expressing VP7-144-eGFP, VP7-177-eGFP or VP7-200-eGFP. At 48 hpi, cells were fixed and prepared for indirect immunofluorescence using guinea pig anti-VP7 primary and TRITC-conjugated secondary antibodies. The first panel represents green eGFP auto-fluorescence, the second panel represents primary antibody recognition (red) and the third panel represents the merged image. Bars, 5 µm.

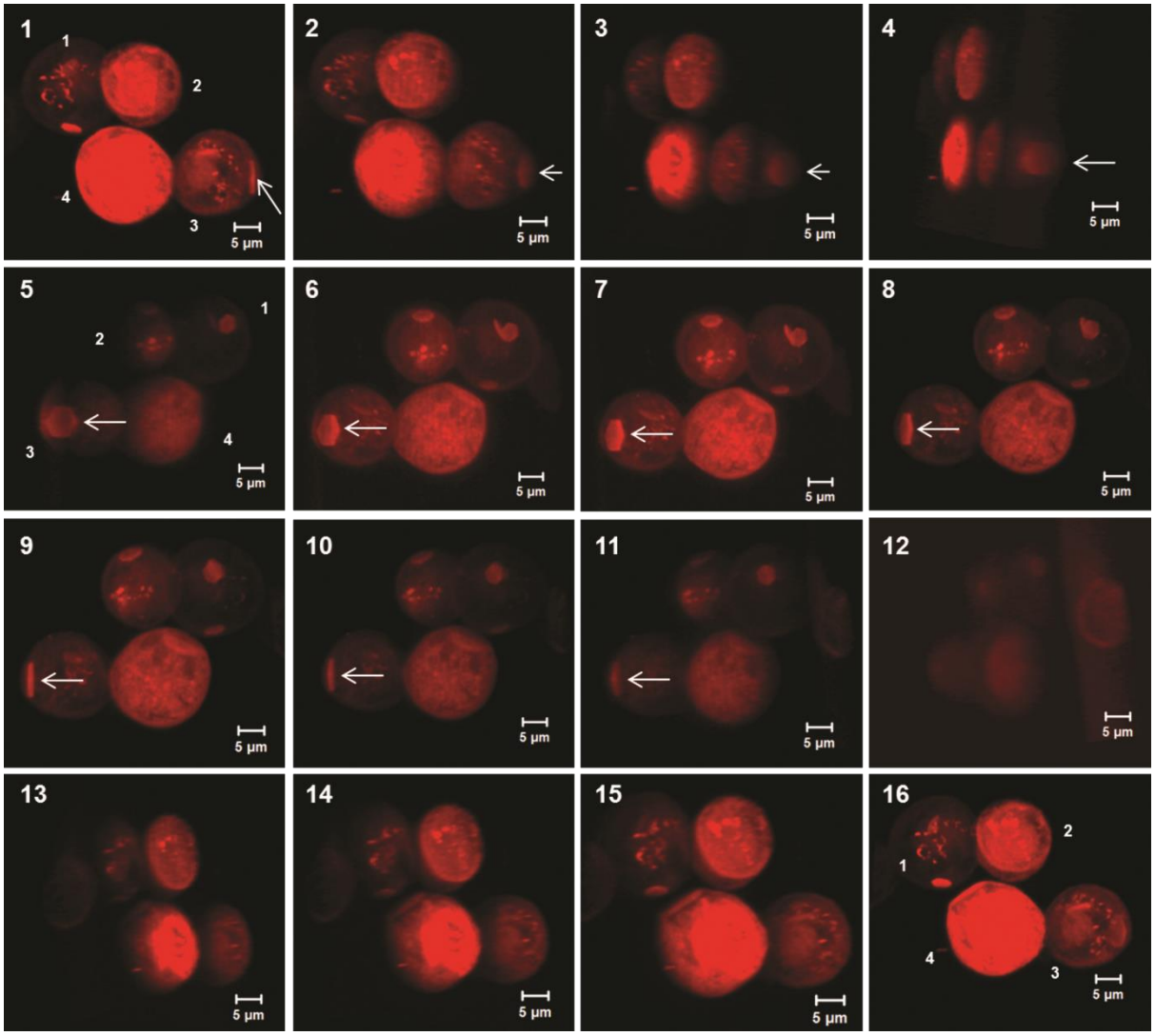

Supplementary Fig. 1. Snapshots of a three-dimensional reconstruction of Sf9 cells infected with a recombinant baculovirus expressing WT VP7 (48 hpi). The reconstruction was rotated around the Y-axis in a clockwise manner, with 90˚ rotation observed in Panel 5, 180˚ in Panel 9, 270˚ between Panels 12 and 13, and 360˚ in Panel 16. Cells are labelled 1 through 4. The particle in cell 3 appeared rod-like at 0˚ (Panel 1) and appeared more hexagonal in nature as the reconstruction was rotated around the Y-axis (Panels 1-8). When viewed at 180˚, the particle was once again viewed as a rod (Panel 9). Cell 1 illustrated that there are often multiple VP7 self-assembly sites per cell. Scale bars represent 5 µm.

REFERENCES

AMIN, S., BARNETT, G.V., PATHAK, J.A., ROBERTS, C.J., SARANGAPANI, P.S. 2014. Protein aggregation, particle formation, characterization & rheology. *Curr. Opin. Colloid Interface Sci.* **19**:438-449.

BASAK, A.K., GOUET, P., GRIMES, J.M., ROY, P., STUART, D. 1996. Crystal structure of the top domain of African horse sickness virus VP7: comparisons with bluetongue virus VP7. *J. Virol.* **70**:3797-3806.

BEKKER, S., HUISMANS, H., VAN STADEN, V. 2014. Factors that affect the intracellular localization and trafficking of African horse sickness virus core protein, VP7. *Virology* **456–457**:279-291.

BOLTE, S. & CORDELIERES, F.P. 2006. A guided tour into subcellular colocalisation analysis in light microscopy. *J. Microsc. (Oxford, U. K.)* **224**:213-232.

BREMER, C.W. 1976. A gel electrophoretic study of the protein and nucleic acid components of African horsesickness virus. *Onderstepoort J. Vet. Res.* **43**:193-199.

BUCCIANTINI, M., GIANNONI, E., CHITI, F., BARONI, F., FORMIGLI, L., ZURDO, J., TADDEI, N., RAMPONI, G., DOBSON, C.M., STEFANI, M. 2002. Inherent toxicity of aggregates implies a common mechanism for protein misfolding diseases. *Nature* **416**:507-511.

BURROUGHS, J.N., O'HARA, R.S., SMALE, C.J., HAMBLIN, C., WALTON, A., ARMSTRONG, R., MERTENS, P.P. 1994. Purification and properties of virus particles, infectious subviral particles, cores and VP7 crystals of African horsesickness virus serotype 9. *J. Gen. Virol.* **75 (Pt 8)**:1849-1857.

CHUMA, T., LE BLOIS, H., SANCHEZ-VIZCAINO, J.M., DIAZ-LAVIADA, M., ROY, P. 1992. Expression of the major core antigen VP7 of African horsesickness virus by a

recombinant baculovirus and its use as a group-specific diagnostic reagent. *J. Gen. Virol.* **73 (Pt 4)**:925-931.

DOBSON, C.M. 2004. Principles of protein folding, misfolding and aggregation. *Semin. Cell Dev. Biol.* **15**:3-16.

GRIMES, J.M., BASAK, A.K., ROY, P., STUART, D. 1995. The crystal structure of bluetongue virus VP7. *Nature* **373**:167-170.

GRIMES, J.M., BURROUGHS, J.N., GOUET, P., DIPROSE, J.M., MALBY, R., ZIENTARA, S., MERTENS, P.P., STUART, D.I. 1998. The atomic structure of the bluetongue virus core. *Nature* **395**:470-478.

HEWAT, E.A., BOOTH, T.F., ROY, P. 1992. Structure of bluetongue virus particles by cryoelectron microscopy. *J. Struct. Biol.* **109**:61-69.

HEYMANN, M.C., RABE, S., RUß, S., KAPPLUSCH, F., SCHULZE, F., STEIN, R., WINKLER, S., HEDRICH, C.M., RÖSEN-WOLFF, A., HOFMANN, S.R. 2015. Fluorescent tags influence the enzymatic activity and subcellular localization of procaspase-1. *Clin. Immunol. (Amsterdam, Neth.)* **160**:172-179.

KAR, A.K., BHATTACHARYA, B., ROY, P. 2007. Bluetongue virus RNA binding protein NS2 is a modulator of viral replication and assembly. *BMC Mol. Biol.* **8**:4.

LORENZO, A. & YANKNER, B.A. 1994. Beta-amyloid neurotoxicity requires fibril formation and is inhibited by congo red. *Proc. Natl. Acad. Sci. U. S. A.* **91**:12243-12247.

MAREE, S., DURBACH, S., HUISMANS, H. 1998. Intracellular production of African horsesickness virus core-like particles by expression of the two major core proteins, VP3 and VP7, in insect cells. *J. Gen. Virol.* **79 (Pt 2)**:333-337.

MAREE, S., MAREE, F.F., PUTTERILL, J.F., DE BEER, T.A.P., HUISMANS, H., THERON, J. 2016. Synthesis of empty african horse sickness virus particles. *Virus Res.* **213**:184-194.

MELLOR, P.S. & HAMBLIN, C. 2004. African horse sickness. *Vet. Res.* **35**:445-466.

MONASTYRSKAYA, K., STAEUBER, N., SUTTON, G., ROY, P. 1997. Effects of domain-switching and site-directed mutagenesis on the properties and functions of the VP7 proteins of two orbiviruses. *Virology* **237**:217-227.

OELLERMANN, R.A., ELS, H.J., ERASMUS, B.J. 1970. Characterization of African horsesickness virus. *Arch. Gesamte Virusforsch.* **29**:163-174.

OLDFIELD, S., ADACHI, A., URAKAWA, T., HIRASAWA, T., ROY, P. 1990. Purification and characterization of the major group-specific core antigen VP7 of bluetongue virus synthesized by a recombinant baculovirus. *J. Gen. Virol.* **71 (Pt 11)**:2649-2656.

REYNOLDS, E.S. 1963. The use of lead citrate at high pH as an electron-opaque stain in electron microscopy. *J. Cell Biol.* **17**:208-212.

ROBERTS, C.J. 2014. Protein aggregation and its impact on product quality. *Curr. Opin. Biotechnol.* **30**:211-217.

ROY, P. 1996. Orbivirus structure and assembly. *Virology* **216**:1-11.

ROY, P., HIRASAWA, T., FERNANDEZ, M., BLINOV, V.M., SANCHEZ-VIXCAIN RODRIQUE, J.M. 1991. The complete sequence of the group-specific antigen, VP7, of African horsesickness disease virus serotype 4 reveals a close relationship to bluetongue virus. *J. Gen. Virol.* **72 (Pt 6)**:1237-1241.

RUTKOWSKA, D.A., MEYER, Q.C., MAREE, F., VOSLOO, W., FICK, W., HUISMANS, H. 2011. The use of soluble African horse sickness viral protein 7 as an antigen delivery and presentation system. *Virus Res.* **156**:35-48.

STEFANI, M. 2004. Protein misfolding and aggregation: new examples in medicine and biology of the dark side of the protein world. *Biochim. Biophys. Acta* **1739**:5-25.

STUDER, D., GRABER, W., AL-AMOUDI, A., EGGLI, P. 2001. A new approach for cryofixation by high-pressure freezing. *J. Microsc. (Oxford, U. K.)* **203**:285-294.

TSUMOTO, K., EJIMA, D., KITA, Y., ARAKAWA, T. 2005. Review: Why is arginine effective in suppressing aggregation? *Protein Pept. Lett.* **12**:613-619.

VENTER, E., VAN DER MERWE, C.F., BUYS, A.V., HUISMANS, H., VAN STADEN, V. 2014. Comparative ultrastructural characterisation of African horse sickness virus-infected mammalian and insect cells reveals novel potential virus release mechanism from insect cells. *J. Gen. Virol.* **95**:642-651.

VERWOERD, D., ELS, H., DE VILLIERS, E., HUISMANS, H. 1972. Structure of the bluetongue virus capsid. *J. Virol.* **10**:783 - 794.

WU, C. & SHEA, J.-E. 2011. Coarse-grained models for protein aggregation. *Curr. Opin. Struct. Biol.* **21**:209-220.